Plotting the Stability Boundary of Cnoidal Waves in Microresonators

Logan Courtright, Zhen Qi, Curtis R. Menyuk
University of Maryland, Baltimore County, 1000 Hilltop Circle, Baltimore, MD, 21250, USA
lcourt1@umbc.edu

Abstract: Previous dynamical methods to map the stability region boundary of cnoidal waves were semi-automatic due to sharp corners. We present a fully automatic method that accounts for corners due to Hopf bifurcations.

OCIS codes: (230.5750) Resonators; (190.5530) Pulse propagation and temporal solitons.

Broadband frequency combs can be created by coupling a laser into a microresonator to create single solitons, but the standard approaches for soliton generation are not deterministic [1, 2].The generation of cnoidal waves is one potential approach, but studying their use requires exploring a large parameter space. Since cnoidal waves must stay stable as the system parameters vary, it is necessary to identify the region in the parameter space where stable solutions exist. Dynamical methods have been developed to find the boundaries of the stable regions, but these methods are only semi-automatic due to sharp corners that appear on the boundary when the instability mechanism changes [2]. Here, we present methods that can continuously track the boundary through a corner in which two different Hopf bifurcations occur.

We first solve the Lugiato-Lefever Equation (LLE) to obtain a cnoidal wave solution. We write the LLE as [3]

$$\frac{\partial \psi}{\partial t} = i\frac{\partial^2 \psi}{\partial x^2} + i|\psi|^2\psi - (i\alpha + 1)\psi + F, \tag{1}$$

where ψ is the field envelope, t is the normalized time, x is the normalized azimuthal coordinate, α is the normalized damping rate, and F is the normalized pump power. We start with a highly stable, stationary cnoidal wave solution. This solution satisfies Eq. (1) with its time derivative set equal to zero,

$$0 = i\frac{\partial^2 \psi}{\partial x^2} + i|\psi|^2\psi - (i\alpha + 1)\psi + F. \tag{2}$$

We then solve Eq. (2) while allowing α and F to vary and examine the stability of the solutions by computationally solving for the set of all eigenvalues $\{\lambda_j\}$ of the linearized LLE [2]. We define $\lambda_j = \rho_j + i\sigma_j$, where $\rho_j = \mathrm{Re}(\lambda_j)$ and $\sigma_j = \mathrm{Im}(\lambda_j)$. Aside from a single eigenvalue always located at zero, all eigenvalues corresponding physically to time in a stable cnoidal wave solution satisfy $\rho_j < 0$. Therefore we look at the maximum ρ_j value of these eigenvalues to determine the stability of the solution. As we allow α and F to vary, we will eventually encounter a stability boundary where the solution will either cease to exist or become unstable. When the solution crosses the stability boundary via a Hopf bifurcation, the real parts of a complex conjugate pair of eigenvalues will cross over the imaginary axis to become positive, and an unstable cnoidal wave solution will continue to exist.

We first reach the stability boundary by increasing F while fixing $\alpha = \alpha_k$ and tracking $\max(\rho_j)$. Eventually we reach a point $c_1 = (\alpha_k, F_1)$ where we cross the stability boundary as the solution becomes unstable via a Hopf bifurcation. As shown in Fig. 1(a), we then use two nearby stable points, $c_2 = (\alpha_k, F_2)$ and $c_3 = (\alpha_k, F_3)$, to find the boundary using quadratic interpolation. At a nearby value of $\alpha = \alpha_{k+1}$, we repeat this method to obtain another point on the stability boundary. This allows us to calculate the slope of the stability boundary $d\alpha/dF$, which then lets us predict the location of the three values of F surrounding the stability boundary at the next value of α, α_{k+2} [4]. We then interpolate to find the actual boundary. In Fig. 1(b), we illustrate this procedure.

When a corner is encountered, the last point on the stability boundary is set as the pivot, with the previous point treated as the endpoint of a line from the pivot of distance r_0 and angle θ_0. We then increase θ relative to θ_0 through the nearby stable region until we reach an point $p_1 = (r_0, \theta_1)$ where a new stability boundary is crossed via a Hopf bifurcation. We then use two nearby stable points, $p_2 = (r_0, \theta_2)$ and $p_3 = (r_0, \theta_3)$, to determine the value of θ where the new stability boundary exists. In Fig. 2(a), we illustrate this procedure, which is analogous to the procedure that we show in Fig. 1(a). At a nearby value of $r = r_1$, we repeat this method to obtain another point on the new stability boundary, then use these values of r and θ to predict the location of the points surrounding the new stability boundary at $r = r_2$. We then follow the new stability boundary further from the corner as shown in Fig. 2(b). As r increases, the angle will deviate from the first calculated value on the boundary when $r = r_0$. Since

this method assumes that the new stability boundary will be relatively straight, we use the θ-value of the predicted points surrounding the boundary at the previous r to verify the boundary location. Once the stability boundary has moved outside of the predicted surrounding points, the corner region is assumed to have been passed and the standard method of interpolation is applied again.

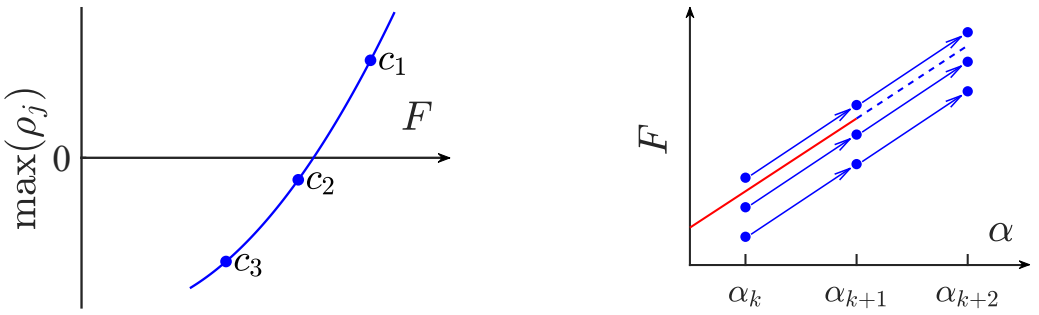

Fig. 1: (a) Quadratic interpolation polynomial constructed from two stable and one unstable cnoidal wave solutions with the same value of α and increasing F. (b) Calculation of the next discretized segment of the stability boundary (dotted-blue line) from the known stability boundary (solid red line) using the predicted points that surround the boundary (blue dots). The blue arrows indicate the predictions.

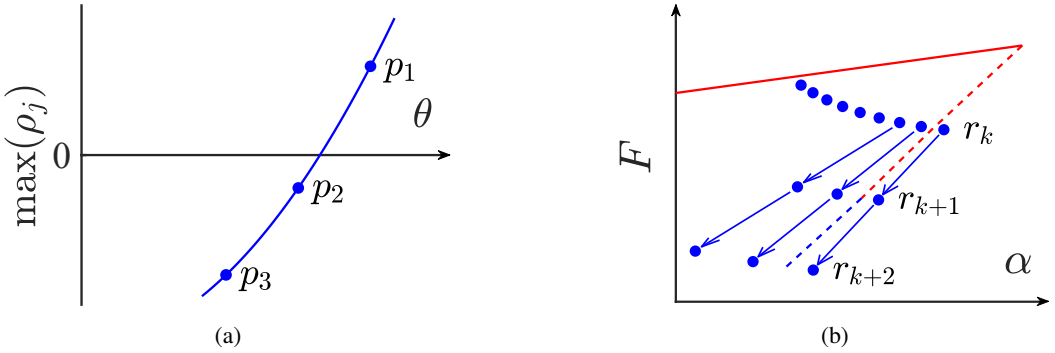

Fig. 2: (a) Quadratic interpolation polynomial constructed from two stable and one unstable cnoidal wave solutions obstained by increasing θ. (b) The location of the new stability boundary (dotted red line) after the corner is found by increasing θ when $r = r_k$ and is indicated by the row of blue dots. The next segment of the new stability boundary (dotted blue line) is found using the predicted points surrounding the boundary

References

1. T. J. Kippenberg,, R. Holzwarth, and S. A. Diddams, "Microresonator-Based Optical Frequency Combs," Science **332**, 555–711 (2015).
2. Z. Qi, S. Wang, J. Jaramillo-Villegas, M. Qi, A. M. Weiner, G. D'Aguanno, T. F. Carruthers, and C. R. Menyuk, "Dissipative cnoidal waves (Turing Rolls) and the soliton limit in microring resonators," Optica **6**, 1220–1232 (2019).
3. Z. Qi, G. D'Aguanno, and C. R. Menyuk, "Nonlinear frequency combs generated by cnoidal waves in microring resonators," J. Opt. Soc. Am. B **34**, 785–794 (2017).
4. S. Wang, A. Docherty, B. Marks, and C. R. Menyuk, "Boundary tracking algorithms for determining the stability of mode-locked pulses," J. Opt. Soc. Am. B **31** 2914–2930 (2014).